Supplementary Information

Table of Content:

Biochemistry of TRAIL-induced apoptosis

TRAIL binds death receptors DR4/5. This promotes the formation of the DISC complex, which is able to recruit and cleave the initiator caspases 8 and 10 (Kischkel et al., 2005). In turn, initiator caspases activate effector caspases such as caspase 3. In most cells, the activity of caspase 3 is blocked by inhibitors (as XIAP), and is relieved only when MOMP (Mitochondrial Outer Membrane Permeabilization) occurs. MOMP is regulated by another pathway involving members of the Bcl2 family, such as Bid, Mcl1, Bax and Bcl2 (Deveraux et al., 1998; Kim et al., 2006; Luo et al., 1998). It can be triggered by initiator caspases via cleavage of Bid, which in turn can activate Bax, which then translocate to the mitochondria, allowing the formation of pores. Smac/Diablo and cytochrome c are released in the cytosol, blocking XIAP inhibitory activity and promoting the formation of the apoptosome (Du et al., 2000; Liu et al., 1996; Verhagen et al., 2000).

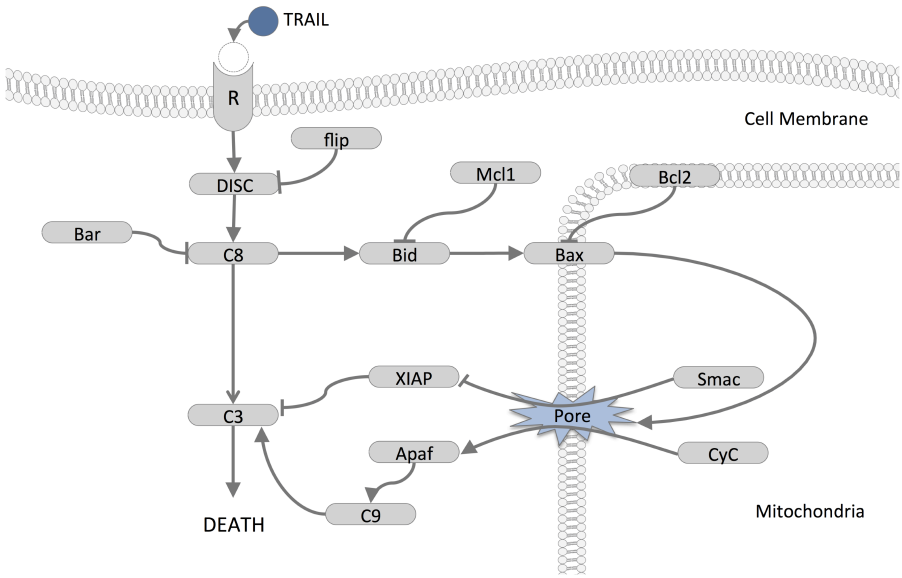

Figure S1. Simplified view on the TRAIL-induced apoptosis pathway The activation of the membrane receptor by TRAIL binding promotes the assembly of the death-inducing signaling complexes (DISC), which recruit and activate initiator caspases like caspase-8 (C8) (Kischkel et al., 1995). Once activated, initiator caspases cleave and activate effector caspases such as caspase-3 (C3). Effector caspases cleave essential structural proteins, inhibitors of DNase, and DNA repair proteins

(PARP), eventually leading to cell death. The cellular effect of effector caspase activation is regulated by factors such as XIAP, which blocks the proteolytic activity of caspase-3 by binding tightly to its active site and promotes its degradation via ubiquitination (Deveraux et al., 1998). In addition to the direct activation of effector caspases, initiator caspases also activate Bid and Bax (Luo et al., 1998). If not kept in check by inhibitors, most notably Bcl2, activated Bax directly contributes to the formation of pores in the mitochondria outer membrane, leading to MOMP (Kim et al., 2006). Following MOMP, critical apoptosis regulators, such as Smac and cytochrome c (CyC), translocate into the cytoplasm. Smac binds to and inactivates XIAP, thus relieving the inhibition of effector caspases by XIAP (Du et al., 2000). Cytochrome c combines with Apaf-1 to form the apoptosome that in turn activates the initiator caspase-9 (C9) that activates effector caspases.

Modeling stochastic protein turnover

We model protein turnover with a stochastic process describing mRNA level fluctuations (promoter activity switches, mRNA production and degradation are stochastic events), and deterministic processes for protein translation and degradation (Figure S2).

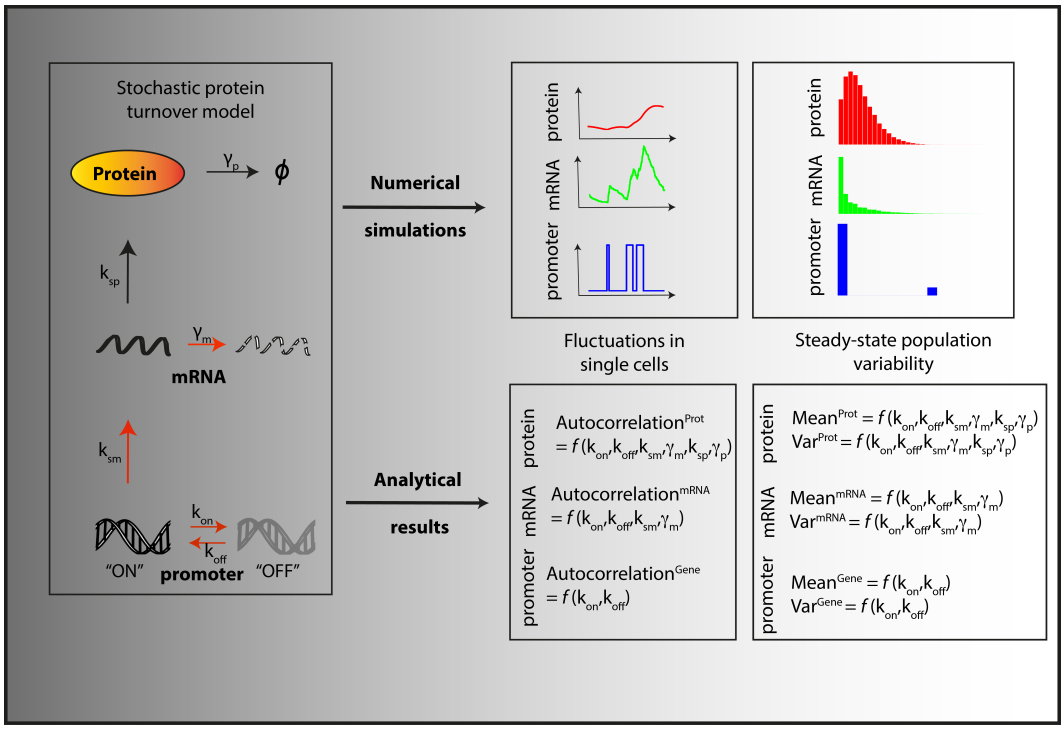

Figure S2. Numerical simulation and analytical characterization of stochastic protein turnover models A stochastic protein turnover model is defined by six rates: the promoter activity switching rates, the mRNA production and degradation rates, the protein per mRNA synthesis rate and the protein degradation rate. Numerical simulations can be used to simulate temporal fluctuations in single cells. When a population of cells is simulated, the cell-to-cell variability can be studied. After some time, cell-to-cell variability reaches a steady state. Analytical calculations on the stochastic protein turnover model provide expressions characterizing the steady-state variability (moments of the steady-state distributions), but also fluctuations (autocorrelation functions). Complete expressions are given elsewhere in supplementary information.

To constrain model rates based on experimentally available information, one can use analytical expressions characterizing steady-state mRNA and protein level distributions (moments) and their fluctuations (autocorrelations functions). The derivation of steady-state distribution moments can be done by performing Laplace transforms on the steady-state formulation of the chemical master equation. The obtained system of equations is closed because there are no reactions of order 2 or higher. To derive autocorrelation, one can combine the set of differential equations connecting the temporal evolution of first moments (closed) with the master equation. Those analytical expressions are:

- Promoter activity (denoted by G, equal to either 0 or 1)
  - $\mathbb{E}[G] = \frac{k_{on}}{k_{on}+k_{off}} = \frac{k_{on}}{\gamma_g} \qquad (\gamma_g = k_{on} + k_{off})$
  - $Var[G] = \mathbb{E}[G](1 - \mathbb{E}[G])$
  - $CV[G]^2 = \frac{Var[G]}{\mathbb{E}[G]^2} = \frac{1-\mathbb{E}[G]}{\mathbb{E}[G]}$
- mRNA level (denoted by m, taking discrete values)
  - $\mathbb{E}[m] = \mathbb{E}[G]\frac{k_{sm}}{\gamma_m}$
  - $Var[m] = \frac{\gamma_m}{\gamma_m+\gamma_g} CV[G]^2\mathbb{E}[m]^2 + \mathbb{E}[m]$
  - $CV[m]^2 = \frac{\gamma_m}{\gamma_m+\gamma_g} CV[G]^2 + \frac{1}{\mathbb{E}[m]}$
- Protein level (denoted by P, taking continuous values)
  - $\mathbb{E}[P] = \mathbb{E}[m]\frac{k_{sp}}{\gamma_p}$
  - $Var[P] = \frac{\gamma_p\gamma_m(\gamma_p+\gamma_m+\gamma_g)}{(\gamma_m+\gamma_p)(\gamma_m+\gamma_g)(\gamma_p+\gamma_g)} CV[G]^2\mathbb{E}[P]^2 + \frac{\gamma_m}{\gamma_m+\gamma_p}\frac{\mathbb{E}[P]^2}{\mathbb{E}[m]}$
  - $CV[P]^2 = \frac{\gamma_p\gamma_m(\gamma_p+\gamma_m+\gamma_g)}{(\gamma_m+\gamma_p)(\gamma_m+\gamma_g)(\gamma_p+\gamma_g)} CV[G]^2 + \frac{\gamma_m}{\gamma_m+\gamma_p}\frac{1}{\mathbb{E}[m]}$
  - $Autoc[\square](t) = e^{-\gamma_p t} + h_m(\gamma_m, \gamma_p, t) + \frac{1}{CV[P]^2}\frac{1-\mathbb{E}[G]}{\mathbb{E}[G]}\frac{\gamma_p\gamma_m}{(\gamma_m+\gamma_g)(\gamma_p+\gamma_g)} h_g(\gamma_g, \gamma_m, \gamma_p, t)$

with:

$h_m(\gamma_m, \gamma_p, t) = \frac{\gamma_p}{\gamma_p-\gamma_m}\{e^{-\gamma_m t} - e^{-\gamma_p t}\}$

$$h_g(\gamma_g,\gamma_m,\gamma_p,t)=\frac{\gamma_p\gamma_m}{(\gamma_p-\gamma_m)(\gamma_m-\gamma_g)(\gamma_p-\gamma_g)}\{(\gamma_m-\gamma_g)e^{-\gamma_p t}+(\gamma_p-\gamma_m)e^{-\gamma_g t}+(\gamma_g-\gamma_p)e^{-\gamma_m t}\}$$

Short-lived protein fluctuations are more sensitive to bursting kinetics

Intuitively, fluctuations of short-lived proteins are expected to be more sensitive to the precise kinetics of bursting than long-lived proteins. Using protein level variability and half-autocorrelation time to characterize protein fluctuations, this hypothesis was confirmed by the corresponding analytical expressions (Figure S3).

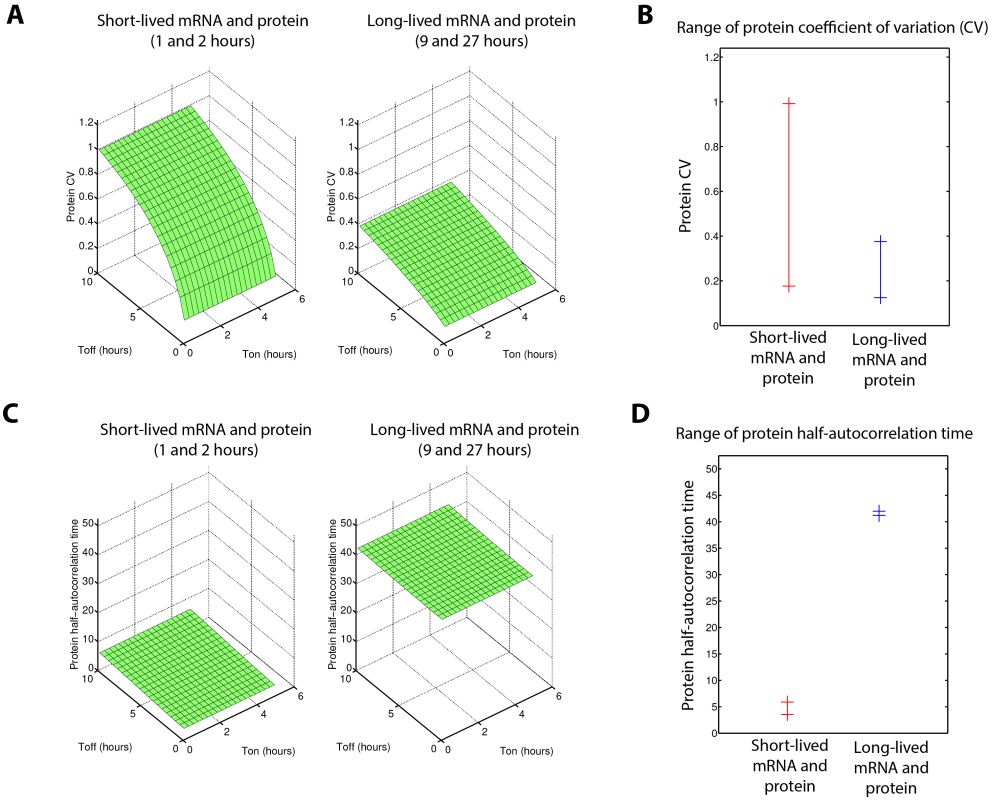

Figure S3. Fluctuations of protein levels caused by transcriptional bursting are exacerbated for short-lived proteins Comparison of protein level coefficient of variation **(A)** and half-autocorrelation time **(C)** as a function of transcriptional bursting rates for two situations: a short-lived protein and mRNA (1 and 2 hours) and a long-lived protein and mRNA (27 and 9 hours). Other rates of the stochastic protein turnover model are chosen such that mean protein and mRNA level are the same (1000 and 17). Combinations of T_{on} and T_{off} values ranging from 0.1 to 5 hours and 0.1 to 10 hours respectively were tested. **(B and D)** Representation of the range of values obtained for all models tested in (A) and (C).

This motivated us to consider standard stochastic protein turnover models for long-lived proteins but to give particular attention to the few short-lived proteins.

Modeling stochastic protein turnover in TRAIL-induced apoptosis

We apply our approach to TRAIL-induced apoptosis. We use EARM kinetic model (Albeck et al., 2008; Spencer et al., 2009) to describe protein-protein reactions taking place between TRAIL death exposure and cell death commitment. It comprises 17 native proteins and 41 other species involved in 71 reactions.

Unless required, we equipped all native proteins with the same default model of stochastic protein turnover. We used median values for mRNA levels, protein and mRNA half-lives from measured distributions in mammalian cells (Schwanhäusser et al., 2011). At the promoter level, switching rates were estimated for a dozen of genes (Suter et al., 2011), we used measured values to constrain model reaction rates. Remaining rates were deduced from the mean and variance of protein level present as initial condition in (Spencer et al., 2009) using analytical expressions derived from the stochastic protein turnover model (Figure S4, Table S1).

As mentioned earlier, short-lived proteins should be given particular attention: transcriptional bursts are smoothed out in the fluctuations of a stable protein while fully revealed when both mRNA and protein exhibit fast turnover. Flip and Mcl1 are known to exhibit very fast turnover (Laussmann et al., 2012; Nijhawan et al., 2003). Measurements in mouse ES cells (Sharova et al., 2009) also suggest that Flip and Mcl1 transcripts are particularly short-lived. Therefore, we considered a specific stochastic protein turnover model for those two proteins, exploring realistic ranges for promoter switching rates, mRNA half-life and protein half-life (Figure S4).

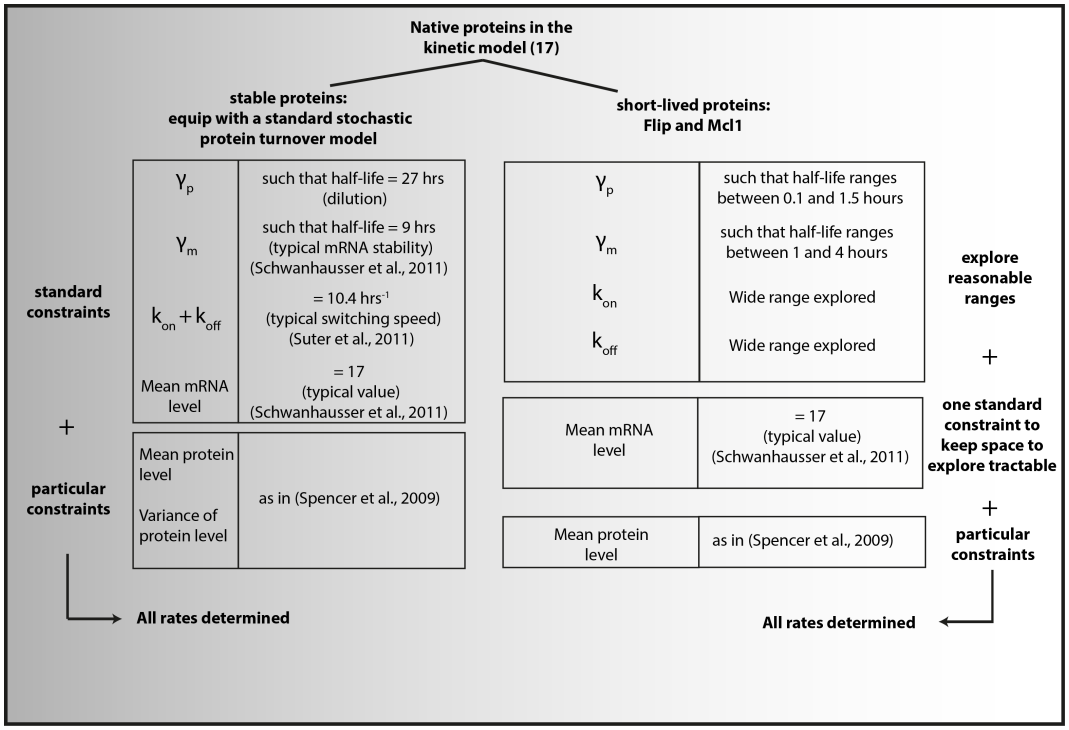

Figure S4. Building stochastic protein turnover models for TRAIL-induced apoptosis Routine followed to choose rates of all 17 native proteins in the EARM kinetic model of TRAIL-induced apoptosis. Typical values from multi-genes studies in mammalian cells are used to constrain rate values. Specific attention is given to Flip and Mcl1 because they are known to be short-lived, and thus more prone to exhibit large variations.

Non-native protein species (catalytically activated forms or complexes) are also subjected to degradation. We used a half-life of 9 hours for TRAIL (as measured by Youn et al., 2007), 1.9 hours for the mitochondrial pores (as in Spencer et al., 2009) and the half-life of the native form for species involving Flip or Mcl1. For all other species we used a unique value (5 hours) to account for the fact that active forms are usually degraded faster (Breitschopf et al., 2000; Ferraro and Pulicati, 2008; Li and Dou, 2000; Tawa et al., 2004; Thorpe et al., 2008 - values recapitulated in Table S3, see dedicated section for discussion on the influence of this choice). We also assumed the feedback loop C3->C6->C8 to be absent (authors comment to Albeck et al., 2008, on editor's website). Otherwise, important cell death was still seen days after TRAIL treatment (see dedicated section for discussion on the feedback loop influence).

Table S1. Standard stochastic protein turnover models

	Constraints	Rate values

Protein	Switching speed $k_{on}+k_{off}$ (hrs^{-1}) [1]	Mean mRNA level [2]	Mean protein level [3]	Protein level Coefficient of Variation [3]	Off to on promoter rate k_{on} (hrs^{-1})	On to off promoter rate k_{off} (hrs^{-1})	k_{sm} (min^{-1})	mRNA deg. rate g_m (hrs^{-1})	Protein synth. rate k_{sp} (min^{-1})	Protein deg. rate g_p (hrs^{-1})
Receptor	10.44	17	1000	0.25	0.388	10.05	0.587	0.077	0.025	0.0257
Caspase-8			10000	0.25	0.388	10.05	0.587		0.25	
Bar			1000	0.25	0.388	10.05	0.587		0.025	
Caspase-3			10000	0.282	0.289	10.15	0.789		0.25	
Caspase-6			10000	0.25	0.388	10.05	0.587		0.25	
XIAP			100000	0.288	0.275	10.17	0.829		2.52	
PARP			1000000	0.25	0.388	10.05	0.587		25.2	
Bid			60000	0.288	0.275	10.17	0.829		1.51	
Bax			80000	0.271	0.318	10.12	0.717		2.01	
Bcl-2			30000	0.294	0.268	10.18	0.871		0.76	
Pore			500000	0.25	0.388	10.05	0.587		12.6	
CytoC_m			500000	0.25	0.388	10.05	0.587		12.6	
Smac			100000	0.25	0.388	10.05	0.587		2.51	
Apaf			100000	0.25	0.388	10.05	0.587		2.51	
Caspase-9			100000	0.25	0.388	10.05	0.587		2.51	

[1]: Suter et al., 2011
[2]: Schwanhäusser et al., 2011
[3]: Spencer et al., 2009

Table S2. Specific stochastic protein turnover models

	Constraints		Rate values					
Protein	Mean mRNA level [2]	Mean protein level [3]	k_{on} (hrs^{-1})	k_{off} (hrs^{-1})	k_{sm} (min^{-1})	g_m (hrs^{-1})	k_{sp} (min^{-1})	g_p (hrs^{-1})
Flip	17	2000	0.0417	0.0625	0.4910	0.6931	3.3978	1.73
Mcl-1	17	20000	0.0417	0.0625	0.4910	0.6931	33.9780	1.73

[1]: Suter et al., 2011
[2]: Schwanhäusser et al., 2011
[3]: Spencer et al., 2009

Table S3. Non-native form degradation

Protein	Half-life (hors)	Reference
TRAIL	9	[4]
Pore*	1.9	[3]
Flip:Receptor	same as Flip	
Mcl-1:tBid	same as Mcl-1	
All others	5	[5]–[9]

[3]: Spencer et al., 2009
[4]: Youn et al., 2007
[5]: Breitschopf et al., 2000
[6]: Ferraro and Pulicati, 2008

[7]: Li and Dou, 2000
[8]: Tawa et al., 2004
[9]: Thorpe et al., 2008

Stochastic protein turnover models predicts transient memory in cell sensitivity to TRAIL and CHX

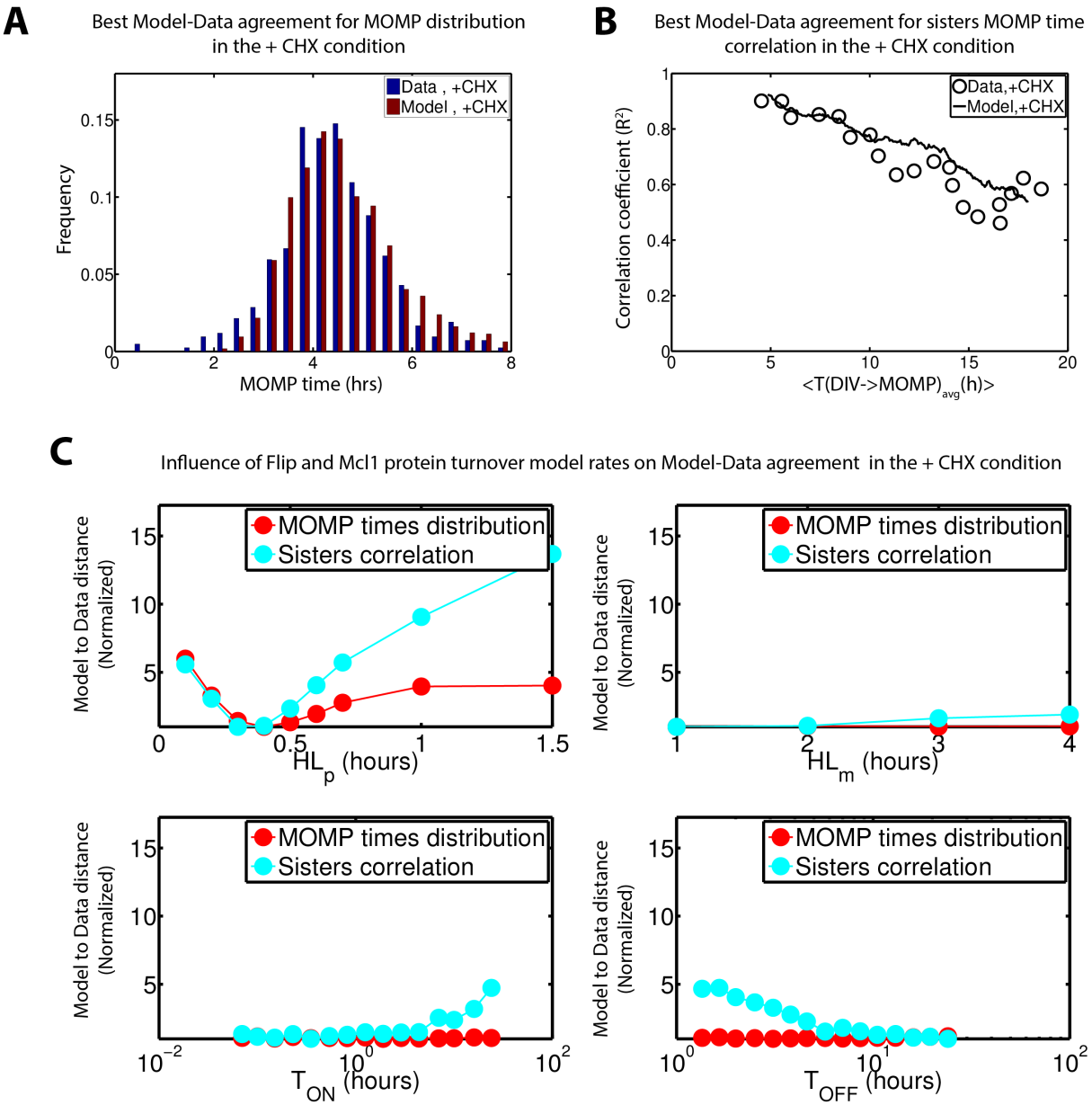

Figure S5. Stochastic protein turnover models captures fluctuations of cell sensitivity to TRAIL and CHX (A) Best found agreement between model and data for MOMP times distribution in the +CHX condition. Obtained for Flip and Mcl1 model rates such that protein/mRNA half-life and mean ON/OFF promoter activity duration equaled 0.4/1 and 1.9/3.1 hours respectively. **(B)** Best found agreement between model and data for MOMP time correlation between sisters in the +CHX condition. Obtained for Flip and Mcl1 model rates such that protein/mRNA half-life and mean ON/OFF promoter activity duration equaled 0.3/1 and 0.35/24 hours respectively. **(C)** Influence of Flip and Mcl1 model rates on Model-Data agreement in the +CHX condition. To read as following:

the best agreement for sister correlation among models such that Flip and Mcl1 protein half-life was 1 hour was ~8 times worse than the best agreement among all models tested.

Large, rare fluctuations of Mcl1 alone is sufficient to explain all observations

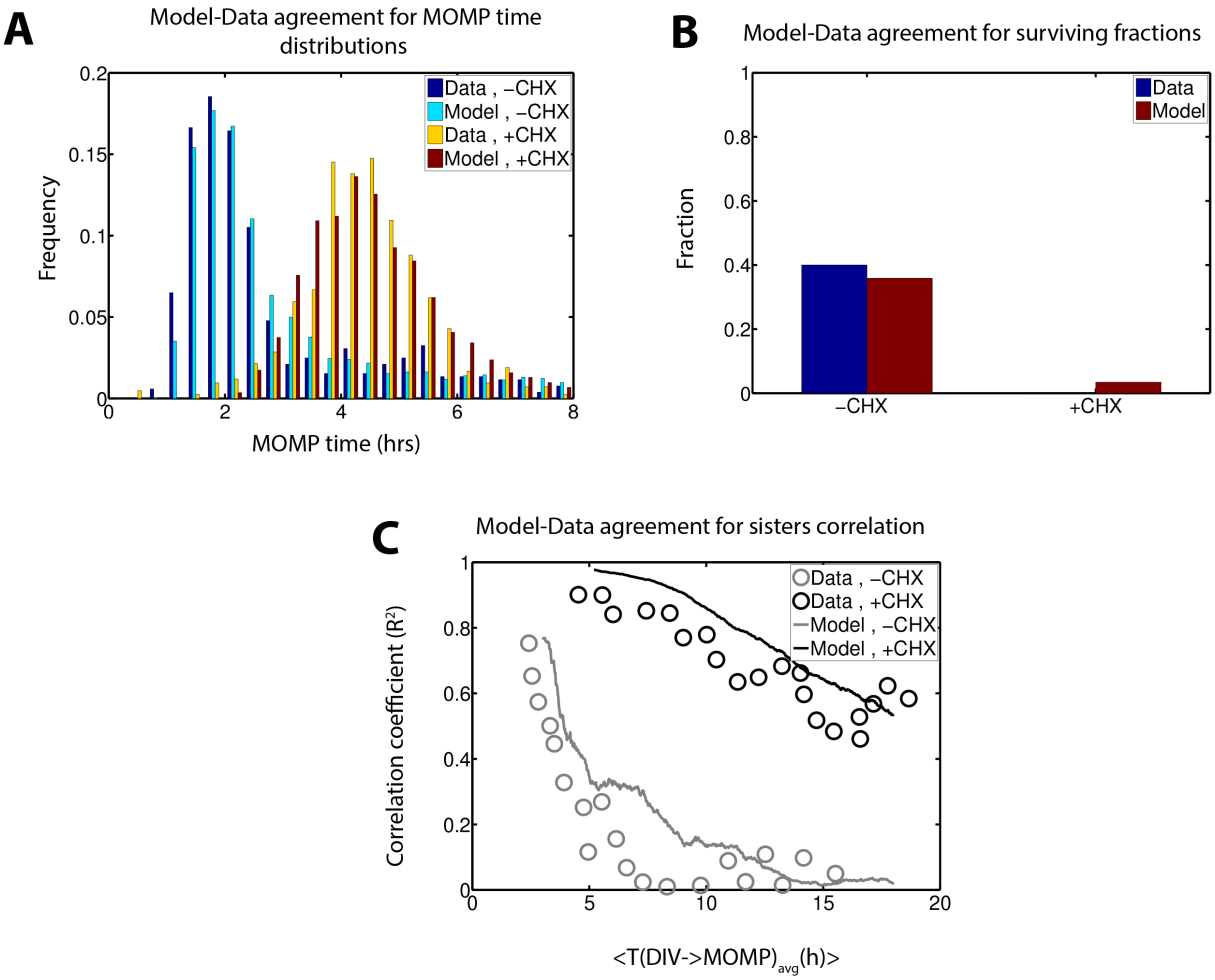

Figure S6. Large, rare fluctuations of Mcl1 alone are sufficient to explain cell fate variability and transient inheritance in both conditions Model-Data agreement for MOMP time distributions **(A)**, surviving fractions **(B)** and sisters correlation of MOMP time **(C)**. While Flip and Mcl1 protein and mRNA half-lives were the same (0.4 and 1.0 hours respectively), only Mcl1 promoter was assumed to have low activity switching rates (16/24 hours mean time ON/OFF). Flip promoter switching rates (0.32/0.14 hours mean time ON/OFF) were chosen such that Flip level coefficient of variation equaled 0.25, as in Spencer et al. (2009).

Influence of C3->C6->C8 feedback loop and of non-native forms degradation

In presence of the feedback loop (as in the original model from Spencer et al., 2009) or with low degradation rates for non-native forms (also as in the original model), model predicts an extinction (or a non-reconstruction) of the cell number at 7 days after the treatment, in contradictions with observations.

Because the functional role of this feedback loop is debated (authors comment to Albeck et al., 2008, on editor's website) and non-native forms are often subjected to active degradation (Breitschopf et al., 2000; Ferraro and Pulicati, 2008; Li and Dou, 2000; Tawa et al., 2004; Thorpe et al., 2008), we investigate whether realistic changes could re-conciliate the model with experimental observations.

We tested the effect of the presence/absence of the feedback loop as well as the influence of the value of the default non-native forms degradation rate (varied in a broad interval, between 2 to 27 hours in half-life). As shown in Figures S7, S8 and S9, model predictions are remarkably robust, with the exception of population reconstruction after 7 days. This criterion led us, in the model, to assume no feedback loop and to use 5 hours as the default half-life of non-native forms.

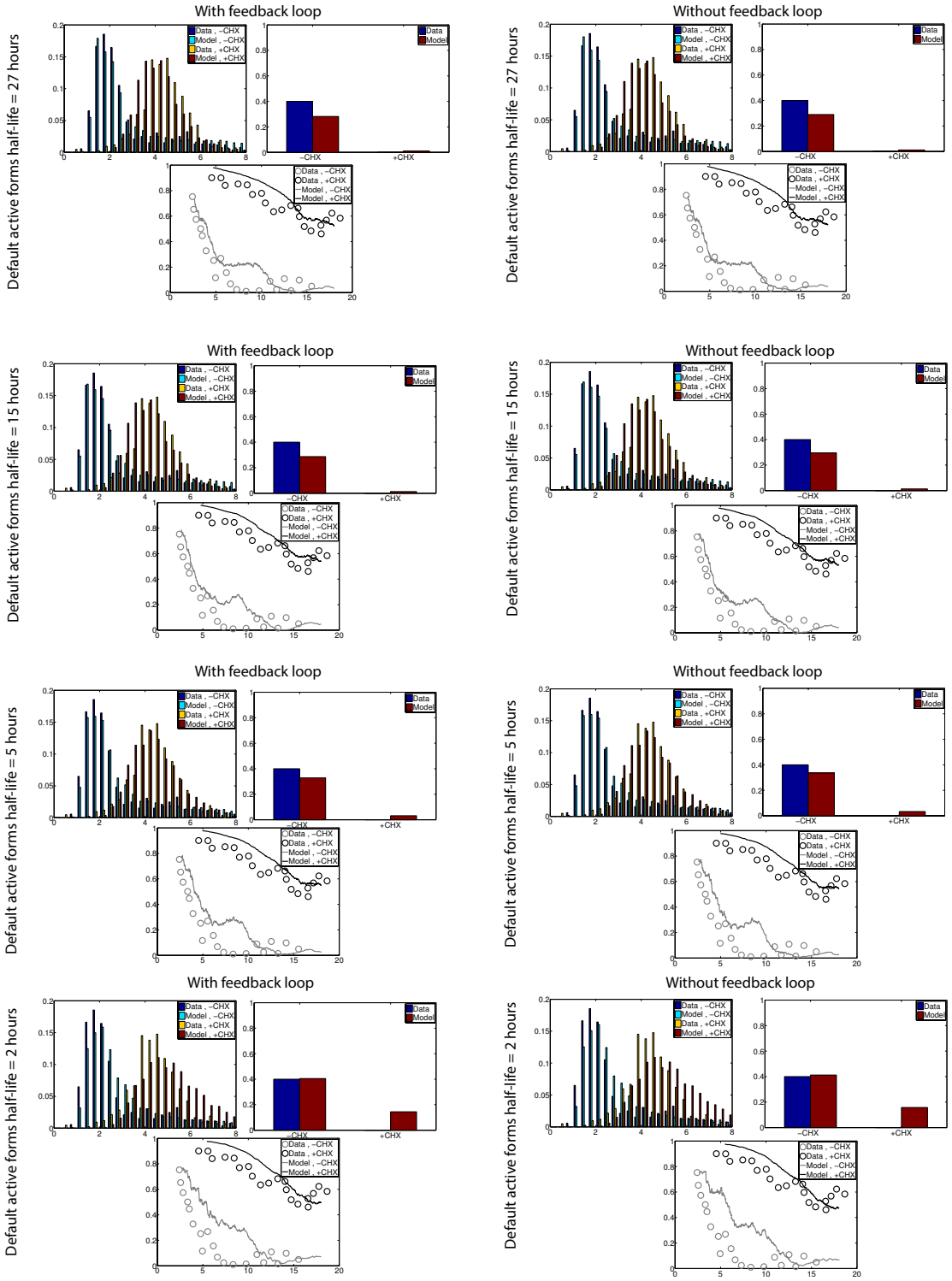

Figure S7. Robustness of short-term model behavior regarding the presence/absence of feedback loop and the degradation of active forms Model-Data agreement is shown for MOMP time distributions, surviving fractions and sisters correlation of MOMP time in both treatment conditions for model variants when the C3->C6->C8 feedback loop is either present/absent and the default active forms half-life is 27, 15, 5 or 2 hours. Significant model-data deviation is seen only for the fastest active forms degradation.

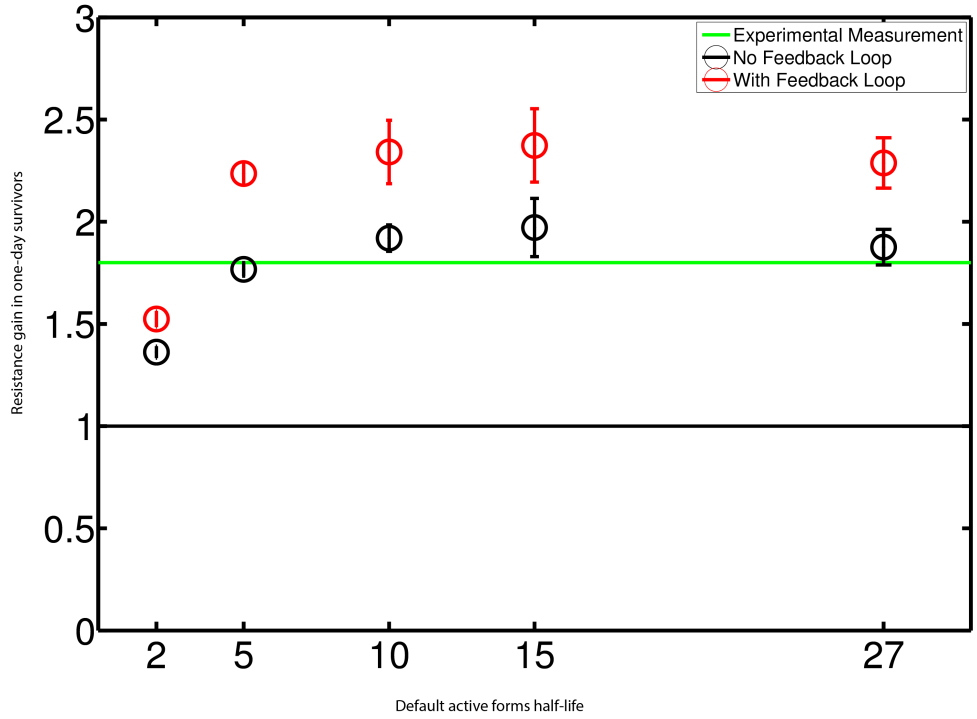

Figure S8. Resistance gain in one day survivors is robust regarding the presence/absence of feedback loop and the degradation of active forms In-silico repeated TRAIL experiment (as in Figure 6) was repeated for model variants regarding presence/absence of the C3->C6->C8 feedback loop and the default active forms half-life. Resistance gain in one-day survivors is shown. Simulations were repeated 4 times with 10^4 cells, error bars indicate standard deviation of estimated resistance gain between replicates.

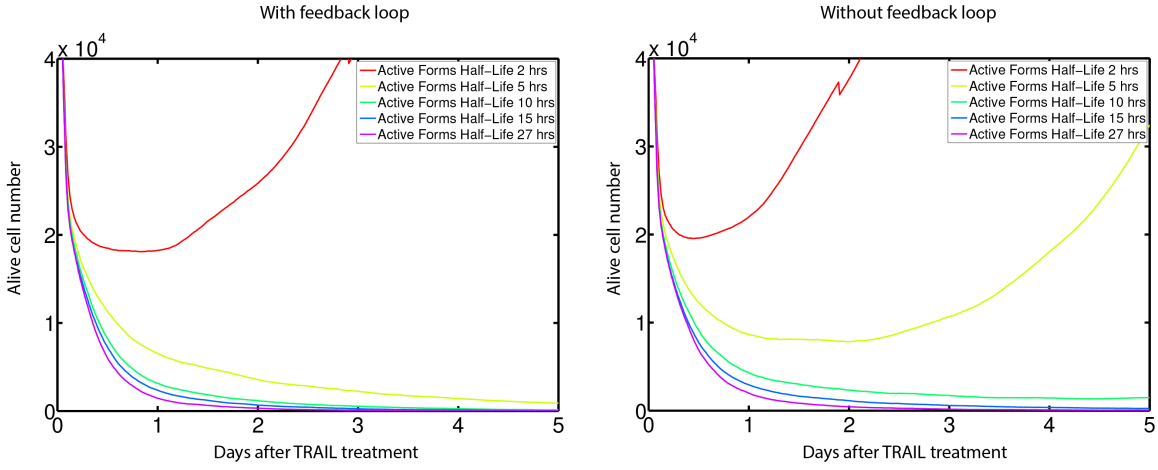

Figure S9. Long-term population survival is not possible with the feedback loop and stable active forms Evolution of alive cell number in populations treated in-silico as in Figure 5, for model several variants regarding presence/absence of the C3->C6->C8 feedback loop and the default active forms half-life.

Supplementary Methods

Simulating TRAIL-induced apoptosis with stochastic protein turnover

In general, the TRAIL signaling protein-protein reactions are taking place in parallel to stochastic protein turnover. When the noise in signaling reactions is neglected due to high protein copy number, those reactions can be simulated using ODEs. However, the rates of protein synthesis is in our model stochastic at it follows mRNA fluctuations.

Promoter activity and mRNA fluctuations were simulated using an implementation of the Gillespie algorithm in C++ (Numerical Recipes). Messenger RNA trajectories were computed and stored in advance because protein levels do not affect the rates of promoter state switches, mRNA production and degradation. The ODEs governing evolution of all protein levels were then simulated using the Semi-Implicit Extrapolation method implemented in C++ (Deuflhard, 1985; Numerical Recipes). This method was significantly faster than a more standard Runge-Kutta method (Dormand-Prince, C++, Numerical Recipes) but gave identical results.

In-silico sister cells experiment

To sample the state (promoter activity, mRNA and protein levels) of the mother cells, all stochastic protein turnover models were simulated during 25 days (Monte-Carlo sampling) for each of the 10^4 (10^5 for results presented in main text) mother cells. This duration was verified by comparison with analytical results to be sufficient to reach the steady-state distribution. Sister cells were simply constructed by duplication of the mother cell state.

Because in experiments from Spencer et al. (2009), the distribution of durations between division and treatment was not uniform (see Figures S5-b and 1-g in Spencer et al., 2009), we applied a sampling algorithm to approximately reproduce those distributions. The overall impact on correlation curves was generally low compared to results obtained with assuming a

fully uniform distribution of division time in the pre-stimulus recording interval. MOMP was considered to have occurred when half of mitochondrial Smac has been released.

In-silico repeated TRAIL experiment

A naïve population of 10^4 cells was obtained as in the sister cells experiment. Each cell was assigned a random time of next division. To account for the fact that the distribution of next division times is not uniform in growing cell populations, we used a distribution obtained by simulating simple growth. New cells were attributed a next division time according to a cell cycle duration normally distributed with 27 hours mean and 3 hours standard deviation. Cells in which cPARP levels exceeded 10^5 were considered dead as in (Gaudet et al. 2012). To closely mimic the experimental protocol used in Flusberg et al. (2013), we accounted for the effect of passing cells by checking population size each day and if needed, removing randomly cells until 10^4 were left. Resistance gain is computed as $RG = \frac{Resistance^{survivors}}{Resistance^{naive\ cells}}$ where $Resistance = \frac{AliveCellNumber(treatment+8hours)}{AliveCellNumber(treatment)}$, similarly to Flusberg et al. (2013).

Quantification of model-data agreement

For the estimation Flip/Mcl1 model rates based cell fate variability experimental data, for the validation against transient cell fate inheritance data and for robustness analysis (Figures 5A-C, 5E), it is needed to quantify the agreement/discrepancy between each model tested and the observed data. Such quantification was performed as follows:

- MOMP time distribution

Data was extracted from Spencer et al. (2009, Figures S4 b and c). It consists in MOMP time histograms (number of cells which did MOMP in a given 20 minutes time interval between 0 and 8 hours after treatment, 24 intervals in total). It was transformed in MOMP time frequencies by dividing by the total cell number. The same MOMP time frequencies were computed from simulated results. An agreement cost was then computed as the squared

deviation between the two sets of frequencies, which respectively represent the empirical/model MOMP time distributions.

- Surviving fraction

An agreement cost for surviving fractions was simply computed as the squared difference between the surviving fractions observed experimentally and in simulations 8 hours after treatment.

- Sister cell MOMP time correlation curve

Spencer et al. (2009) quantified the transient inheritance of MOMP times by computing a curve of sister cells MOMP time correlation as follows: pairs of sister cells for which both cells did MOMP before 8 hours were sorted as a function of the average time between division and MOMP, and linear regression correlation coefficients were computed for all groups obtained by sliding a window of constant size along the sorted pairs. For each group, mean time between division and MOMP was also computed, thus providing the abscissa of the corresponding point in the curve. From this data (Figures S5-d in Spencer et al., 2009), twenty representative points were extracted. To compute a comparable curve from simulations results, we applied the same quantification of sister cell MOMP time correlations. The group size was chosen such that fraction of total pairs in each group is 10%, similarly to what has been done in Spencer et al. One should not that the correlation values are available at different time points between the experimental and simulated curves. Thus, to permit a quantification of the agreement cost, each point in the experimental curve was mapped to the point in the simulated curve for which time points are the closest. The cost then penalizes, for each pair of points, a difference in the correlations but also in the time. In a formal manner, if for each point i in the data curve, the point $j = closestDivToMOMP_i$ in the simulated curve such that $DivToMOMP_j^{simulation}$ is the closest to $DivToMOMP_i^{data}$, the cost is then computed as:

$$cost = \sum(Corr_i^{data} - Corr_{closestDivToMOMP(i)}^{simulation})^2 + \sum(DivToMOMP_i^{data} - DivToMOMP_{closestDivToMOMP(i)}^{simulation})^2$$

- Comparison between the different types of data

To permit comparison between the different types of data, in each case a threshold for the cost defining agreement/disagreement was manually set by visual comparison of experimental and simulated data. For visualization purposes, Figures 4-A,B,E represent a linearly normalized cost such that the threshold value correspond to 0.5 (represented in yellow). Normalized costs above 1 are capped to 1 and represented in red. The threshold costs used were 0.02/0.02, 0.01/0.01, and 2/2.5 for MOMP time distributions, surviving fractions and sister cell correlations respectively (TRAIL+CHX condition/TRAIL alone condition). To assign an agreement cost for MOMP time distribution AND surviving fractions (Figure 4C), the maximum of the two normalized costs is taken.

Supplementary References

Breitschopf, K., Zeiher, a M., and Dimmeler, S. (2000). Ubiquitin-mediated degradation of the proapoptotic active form of bid. A functional consequence on apoptosis induction. J. Biol. Chem. *275*, 21648–21652.

Deveraux, Q.L., Roy, N., Stennicke, H.R., Van Arsdale, T., Zhou, Q., Srinivasula, S.M., Alnemri, E.S., Salvesen, G.S., and Reed, J.C. (1998). IAPs block apoptotic events induced by caspase-8 and cytochrome c by direct inhibition of distinct caspases. EMBO J. *17*, 2215–2223.

Deuflhard, P. (1985). Recent Progress in Extrapolation Methods for Ordinary Differential Equations. *SIAM Review*, *27*(4), 505–535. doi:10.1137/1027140

Du, C., Fang, M., Li, Y., Li, L., and Wang, X. (2000). Smac, a mitochondrial protein that promotes cytochrome c-dependent caspase activation by eliminating IAP inhibition. Cell *102*, 33–42.

Ferraro, E., and Pulicati, A. (2008). Apoptosome-deficient cells lose cytochrome c through proteasomal degradation but survive by autophagy-dependent glycolysis. Mol. Biol. Cell *19*, 3576–3588.

Kim, H., Rafiuddin-Shah, M., Tu, H.-C., Jeffers, J.R., Zambetti, G.P., Hsieh, J.J.-D., and Cheng, E.H.-Y. (2006). Hierarchical regulation of mitochondrion-dependent apoptosis by BCL-2 subfamilies. Nat. Cell Biol. *8*, 1348–1358.

Kischkel, F.C., Hellbardt, S., Behrmann, I., Germer, M., Pawlita, M., Krammer, P.H., and Peter, M.E. (1995). Cytotoxicity-dependent APO-1 (Fas/CD95)-associated proteins form a death-inducing signaling complex (DISC) with the receptor. EMBO J. *14*, 5579–5588.

Laussmann, M. a, Passante, E., Hellwig, C.T., Tomiczek, B., Flanagan, L., Prehn, J.H.M., Huber, H.J., and Rehm, M. (2012). Proteasome inhibition can impair caspase-8 activation upon submaximal stimulation of apoptotic tumor necrosis factor-related apoptosis inducing ligand (TRAIL) signaling. J. Biol. Chem. *287*, 14402–14411.

Li, B., and Dou, Q.P. (2000). Bax degradation by the ubiquitin/proteasome-dependent pathway: involvement in tumor survival and progression. Proc. Natl. Acad. Sci. U. S. A. *97*, 3850–3855.

Liu, X., Kim, C.N., Yang, J., Jemmerson, R., and Wang, X. (1996). Induction of apoptotic program in cell-free extracts: requirement for dATP and cytochrome c. Cell *86*, 147–157.

Luo, X., Budihardjo, I., Zou, H., Slaughter, C., and Wang, X. (1998). Bid, a Bcl2 interacting protein, mediates cytochrome c release from mitochondria in response to activation of cell surface death receptors. Cell *94*, 481–490.

Schwanhäusser, B., Busse, D., Li, N., Dittmar, G., Schuchhardt, J., Wolf, J., Chen, W., and Selbach, M. (2011). Global quantification of mammalian gene expression control. Nature *473*, 337–342.

Sharova, L. V, Sharov, A. a, Nedorezov, T., Piao, Y., Shaik, N., and Ko, M.S.H. (2009). Database for mRNA half-life of 19 977 genes obtained by DNA microarray analysis of pluripotent and differentiating mouse embryonic stem cells. DNA Res. *16*, 45–58.

Tawa, P., Hell, K., Giroux, A., and Grimm, E. (2004). Catalytic activity of caspase-3 is required for its degradation: stabilization of the active complex by synthetic inhibitors. Cell Death Differ. 439–447.

Thorpe, J., Christian, P., and Schwarze, S. (2008). Proteasome Inhibition Blocks Caspase-8 Degradation and Sensitizes Prostate Cancer Cells to Death Receptor-Mediated Apoptosis. Prostate *209*, 200–209.

Verhagen, a M., Ekert, P.G., Pakusch, M., Silke, J., Connolly, L.M., Reid, G.E., Moritz, R.L., Simpson, R.J., and Vaux, D.L. (2000). Identification of DIABLO, a mammalian protein that promotes apoptosis by binding to and antagonizing IAP proteins. Cell *102*, 43–53.

Youn, Y.S., Shin, M.J., Chae, S.Y., Jin, C.-H., Kim, T.H., and Lee, K.C. (2007). Biological and physicochemical evaluation of the conformational stability of tumor necrosis factor-related apoptosis-inducing ligand (TRAIL). Biotechnol. Lett. *29*, 713–721.